Force Field Development and MD Simulations of Poly(ethylene oxide)/$LiBF_4$ Polymer Electrolytes

Oleg Borodin,*,† Grant D. Smith,†,‡ and Richard Douglas†

Department of Materials Science and Engineering, 122 S. Central Campus Drive, Rm. 304, University of Utah, Salt Lake City, Utah 84112, and Department of Chemical and Fuels Engineering, University of Utah, Salt Lake City, Utah 84112

Received: November 22, 2002; In Final Form: April 14, 2003

Quantum chemistry-based force fields with many-body polarizable interactions and two-body effective polarizability parameters have been developed for the interaction of poly(ethylene oxide) (PEO) with Li^+ and BF_4^-. The Li^+/ether repulsion parameters were found to be transferable to another polyether, such as poly(methylene oxide), that is interacting with a Li^+ cation. Molecular dynamics (MD) simulations have been performed for PEO ($M_w = 2380$)/$LiBF_4$ for EO:Li = 15:1 at three temperatures: 363, 393, and 423 K. The Li^+ environment was found to be in reasonable agreement with that measured for other lithium salts that have been doped in PEO. MD simulations employing the many-body (MB) polarizable force field predicted ion conductivity, self-diffusion coefficients, and the slowing of the PEO dynamics upon the addition of $LiBF_4$ salt that were in good agreement with experiments. MD simulations employing the two-body (TB) force field yielded polymer and ion dynamics that were slower than those from the simulations employing the MB force field. Analysis of the Li^+ cation diffusion mechanism revealed that the Li^+ cations with significant motion along PEO chains have a much higher self-diffusion coefficient than do the Li^+ cations that do not undergo a noticeable motion along PEO chains, which suggests that the Li^+ motion along PEO makes an important contribution to the cation diffusion mechanism.

I. Introduction

Solid polymer electrolytes (SPEs) are ionically conducting, solvent-free materials that are usually composed of alkali salts dissolved in a polymer matrix. They combine an ease of fabrication, good mechanical and electrochemical stability, and low flammability and toxicity with the ability to form good interfacial contact with electrodes.[1,2] These factors position SPEs among the best candidates for use in secondary lithium batteries for automotive, aerospace, and portable electronics applications. Significant progress has been made toward understanding the structure and transport properties of SPEs. Conductivity in semicrystalline SPEs was shown to be due to an amorphous phase[3] where dynamic pathways for Li^+ transport are created.[1] The Li^+ cation in the amorphous phase was found to be coordinated by 3−6 ether oxygen (EO) atoms from one or two chains (or segments of the same chain), which is similar to cation coordination in crown ethers.[4,5] A dynamic percolation model[6,7] was developed to describe cation transport through a disordered polymer phase qualitatively. In the simple realization of the model, cation motion is described by the hopping time along the pathways and renewal time for the pathway to open.[7] This model was successful in interpreting experimental data in terms of these two characteristic time scales (hopping time and renewal time).[7,8] However, a recent report of the high ionic conductivity in crystalline PEO/$LiSbF_6$ and PEO/$LiPF_6$ indicated that cation transport also can occur in a crystalline phase for some polymer−salt complexes, further complicating the understanding of SPEs. The cation transport mechanism in technologically important comb-branched copolymers with ethylene oxide side chains was found to be relatively independent of the polymer framework,[9] whereas the ionic conductivity of the polymer electrolyte was found to increase as the molecular weight of the side chains increased, reaching a plateau at 6−7 EO atoms,[10] coinciding with the number of EO atoms that are required for wrapping around a Li^+ cation.[4] Despite all the experimental insight into ion transport in SPEs, a fundamental molecular level understanding of the structure−property relationship in SPEs is still missing.

Molecular dynamics (MD) simulations are well suited for studying structure on the nanometer length scale and dynamics on the scale from subpicoseconds to tens of nanoseconds, positioning them as ideal candidates for the study of cation environment and transport in SPEs. The first comprehensive MD simulations study of PEO/LiI[11,12] indicated that PEO acted as a polydentate ligand, wrapping around the Li^+ cation and allowing Li^+ transport along the PEO segments, hopping from one segment to another, and associating−dissociating with anions. The influence of the addition of lithium salt on the PEO conformations and dynamics was also thoroughly discussed.[11,12] Despite the insight provided by the previous studies,[11,12] the dominant mechanism for cation transport in high-molecular-weight polymer electrolytes is not completely resolved. Little attention was also given to exploration of the ability of MD simulations with the "off-the-shelf" force field to predict structural and dynamic properties. Moreover, when the off-the-shelf potentials were used for the PEO/LiI simulations, the ions did not move on the nanosecond time scale, forcing authors to made ad hoc modifications of the potential.[12] The MD simulations of NaI[13] with the force field parameters tuned to reproduce

* Author to whom correspondence should be addressed. E-mail: Oleg.Borodin@utah.edu.
† Department of Materials Science and Engineering.
‡ Department of Chemical and Fuels Engineering.

10.1021/jp027539z CCC: $25.00
Published on Web 06/24/2003

PEO and PEO/NaI crystal structures yielded information about the structure and dynamics of those SPEs that was qualitatively similar to that found for the PEO/LiI SPEs.[11,12] A modified all-atom potential for PEO/NaI was used in simulations by the de Leeuw group,[14] leading to a phase separation and forcing the authors to reduce ion charges by one-half to facilitate ion motion. Halley's group[15] investigated the temperature dependence of ion aggregation in SPEs, employing the two-body (TB) quantum chemistry-based force field,[16] whereas the Wheeler group performed comprehensive MD simulations, combined with the spectroscopic measurements study of the tetraglyme/$LiCF_3SO_3$ structure.[17] Their simulations with the AMBER 5 TB force field predicted local anion environments, which was in good agreement with the spectroscopic measurements if the Li^+−triflate coordination cutoff was set to 2 Å; however, no ion transport properties have been investigated.

Our previous MD simulations[4,18] with the quantum chemistry-based force field[19] for short PEO chains ($M_w = 530$) that were doped with LiI predicted the Li^+ environment to be similar to that for crown ether, with 3−6 EO atoms coordinated around a Li^+ cation, which is in good agreement with neutron diffraction with isotopic substitution (NDIS) experiments, validating the ability of the force field to predict Li^+ complexation accurately.[4] Because of low PEO molecular weight ($M_w = 530$), the dominant mechanism of cation diffusion in that system was Li^+ motion, together with PEO oligomers; however, Li^+ motion along the chains with occasional interchain hopping was observed, which is in agreement with the Li^+ transport mechanism that has been observed for the high-molecular-weight PEO/LiI.[12] The structural and dynamic properties of PEO away from the first coordination shell of Li^+ were found to be similar to those in bulk PEO, whereas the PEO segments in the Li^+ first coordination shell exhibited conformational populations and dynamics (different from those of the bulk PEO) that were only slightly dependent on salt concentration, allowing one to view polymer electrolyte as a composite of pure PEO-like domains and PEO−salt-rich domains. Similar features were observed in MD simulations of PEO ($M_w = 530$)/$LiPF_6$.[20]

On the basis of previous MD simulations and experimental studies of SPEs, we conclude that the Li^+ cation environment is understood rather well, whereas the dominant cation diffusion mechanism in high-molecular-weight SPEs is not completely resolved and must be studied further. The majority of the force fields for PEO-based SPEs were quite often, at best, qualitative,[11−16] casting doubt on the validity of the results and indicating no predictive capabilities. Moreover, many groups used the two-body nonpolarizable potentials[11−17] for simulations of polymer electrolytes, despite the polarizability being acknowledged to be important for accurate prediction of the structure[4] and dynamics.[21] Attempts to include polarizability in a form of the TB effective polarizable force field were rather successful for prediction of the cation environment; however, the ion dynamics and conductivity were found to be up to an order of magnitude slower, in comparison to experiments.[4,18,20] A caveat of the previously used methodology for developing the two-body effective polarizable potentials[19] is that the effects of the condensed phase are estimated on the basis of the gas-phase calculations of small Li^+/ether clusters without any anions present; this is a situation that occurs only for "free" Li^+ cations, which constitute only 10%−60% of the total number of cations. Usage of the many-body (MB) polarizable force fields, on the other hand, is the most rigorous and elegant approach to the problem of accurate force field development for SPEs, because it naturally considers the many-body nature of the polarizable interactions that account for most of the condensed-phase effects in SPEs.

This paper is the third paper of a three-paper series[22,23] that examines and discusses methods for the systematic development of the TB and MB force fields for polymer melts and polymer electrolytes, force field validation, and studies of the mechanism of ion transport in polymer electrolytes. In the previous two papers,[22,23] we have presented a systematic methodology for developing the MB polarizable and TB nonpolarizable quantum chemistry-based force fields for PEO. We have developed three force fields: FF-1, FF-2, and FF-3.[22] The FF-1 force field contained a set of charges that described the electrostatic potential around PEO oligomers well at intermediate (3−5 Å) separations from the molecule but underestimated the electrostatic potential in the proximity of EO atoms, where Li^+ complexation is expected to be important. The FF-2 and FF-3 force fields contained a set of charges that adequately described the electrostatic potential in the proximity of EO atoms but overestimated the electrostatic potential farther from a molecule. The FF-1 and FF-2 force field were quantum chemistry-based potentials with no adjustable parameters, whereas the FF-3 force field contains a torsional potential with lowered barriers for conformational transitions. MD simulations were performed on PEO and its oligomers using all these force fields.[23] The many-body polarizable interactions were found to have little influence on the PEO dynamics and slightly increased the populations of tgt and tgg conformers.[23] MD simulations using the FF-1 and FF-3 force fields yielded thermodynamic properties (density, heat of vaporization), static structure factors, characteristic ratios, conformational populations, oligomers self-diffusion coefficients, incoherent intermediate structure factors, frequency-dependent dielectric constants and dielectric losses, and ^{13}C spin−lattice relaxation times (T_1) that were in good agreement with the experiments, whereas the FF-2 force field exhibited slower dynamics than the FF-1 and FF-2 force fields and the experiments.[23]

In this paper, we develop the MB polarizable and TB force fields for PEO/$LiBF_4$ polymer electrolytes. The outline of this paper is as follows. In Section II, we summarize evidence from the previous MD simulations that the many-body polarizability effects are important for accurate prediction of the structure and dynamics in polymer electrolytes. Derivation of the quantum chemistry-based force with many-body polarizable and two-body effective polarizability terms for Li^+/BF_4^-/ether clusters is presented in Section III, along with the necessary quantum chemistry calculations. The MD simulation methodology, and the results of MD simulations of PEO/$LiBF_4$ SPEs, are presented and discussed in Section IV.

II. Importance of Polarizable Interactions for Li^+ Complexes with Anions and Poly(ethylene oxide)

This section presents evidence of the importance of the inclusion of polarization interactions in the force fields for SPEs. Our previous quantum chemistry study[20] of Li^+/PF_6^- interactions showed that the polarizable interaction accounted for ∼40−50 kcal/mol of the Li^+/PF_6^- total complexation energy of approximately −130 kcal/mol. Investigation of a unit charge interaction with dimethyl ether and dimethoxyethane (DME)[22] indicated that the many-body polarization energy is comparable to the electrostatic potential at Li−O separations of ∼2 Å,[19] which is approximately the position of the first peak of the Li−O radial distribution function (RDF) in the PEO/LiI solutions obtained from the joint MD simulations and NDIS study.[4] MD simulations of PEO/NaI indicated that inclusion of the polariza-

TABLE 1: Li^+/BF_4^- Complex Energy and Li−B Separations (r_{Li-B})

level of theory	BF_4^- basis set	Li^+ basis set	r_{Li-B} (Å)	complex energy (kcal/mol)
		C_{3V}^{Li-3F}		
HF	aug-cc-pvDz	[5s2p1d]	MP2geom	−140.1
	aug-cc-pvDz	[5s2p2d]	MP2geom	−141.8
MP2(full)	aug-cc-pvDz	[5s2p1d]	2.08	−139.2
	aug-cc-pvDz	[5s2p2d]	2.06	−143.1
B3LYP	aug-cc-pvDz	[5s2p1d]	2.07	−140.8
	aug-cc-pvTz	[5s2p1d]	2.06	−141.5
	aug-cc-pvDz	[5s2p2d]	2.06	−143.9
	aug-cc-pvTz	[5s2p2d]	2.06	−143.0
B3PW91	aug-cc-pvDz	[5s2p2d]	2.06	−142.7
	aug-cc-pvTz	[5s2p2d]	2.06	−141.7
		C_{2V}		
B3PW91	aug-cc-pvDz	[5s2p2d]	2.32	−144.0
		C_{3V}^{Li-1F}		
B3PW91	aug-cc-pvDz	[5s2p2d]	3.19	−126.2

tion interactions slows the polymer dynamics.[21] On the basis of this evidence, we conclude that the previous MD simulations and quantum chemistry studies suggest that inclusion of the polarization interaction is important for accurate prediction of the properties of SPEs in MD simulations.

Our previous force fields[19,20] accounted for many-body polarizable interactions in a mean-field sense by adding effective two-body polarization terms that are based on gas-phase quantum chemistry calculations. Here, we take a more rigorous approach and develop a PEO/$LiBF_4$ force field that includes the many-body polarization interactions explicitly. We then perform MD simulations of the PEO/$LiBF_4$ solutions and investigate the possibility of approximating many-body polarizable interactions with the two-body effective polarizability terms. Hence, unlike previous work,[19,20] we obtain the two-body effective polarizability parameters from condensed-phase simulations rather than from the gas-phase studies of Li^+/ether clusters.

III. Quantum Chemistry Studies and Force Field Development

A. Li^+/BF_4^- Complex. In our previous studies,[19] we found that the standard double-ζ (D95[24]) and triple-ζ split valence (6-311G[25]) basis sets and their augmentations gave poor descriptions of Li^+ in LiCl and LiI, because of their poor description of Li^+ 1s electrons. This is manifested by large basis set superposition errors (BSSEs) (>3 kcal/mol) and poor computed dissociation energies for these diatomic molecules.[19] A new Li^+ basis set of the [8s4p3d/5s3p2d] type with an improved description of 1s electrons was derived.[19] This basis set was used in quantum chemistry studies of LiCl and LiI, which yielded complex energies and bond lengths of LiCl and LiI that were in good agreement with the existing experimental data.[19] It was also found, for the case of I^- in LiI, which is a large diffuse anion, that the use of a smaller Li basis set [5s2p1d] could adequately reproduce the LiI complex energy and geometry, but for Cl^-, which is a relatively small anion, the larger [5s3p2d] basis set had to be utilized.

Following our studies of ethylene oxide oligomers, we use the aug-cc-pvXz (X = D, T) basis sets for BF_4^-, together with the previously developed [5s2p1d] and [5s3p2d] basis sets for Li^+. The Gaussian 98 package[26] was used for all quantum chemistry calculations. The effect of the level of theory was investigated by calculating the Li^+/BF_4^- complex energy at the Hartree−Fock (HF) and Møller−Plesset second-order (MP2) levels and using the B3LYP and B3PW91[27] density functionals for the Li^+/BF_4^- complex of C_{3v} symmetry, with the Li^+ cation interacting strongly with three fluorine atoms (denoted at C_{3v}^{Li-3F} and shown in Figure 1). The complex energy of Li^+/BF_4^- was defined as the energy of the optimized complex minus the energy of the isolated Li^+ and BF_4^- and is shown in Table 1. All levels of theory yield a value of the Li^+/BF_4^- complex energy in the range from −139.2 kcal/mol to −143.9 kcal/mol, with Li−B separations of 2.06−2.08 Å. The BSSE corrections were <0.15 kcal/mol for the B3LYP density functional and 0.60 for the MP2 level using aug-cc-pvDz basis set for BF_4^- and [5s2p1d] for Li^+. Because of the small magnitude of the BSSE for the Li^+/BF_4^- complex, we do not correct the Li^+/BF_4^- complex energies for BSSE from this point forward. The addition of extra d- and p-functions to the Li^+ [5s2p1d] basis set increased the absolute value of the Li^+/BF_4^- complex energy by 1.7−3.9 kcal/mol and decreased the Li−B separation up to 0.02 Å. Increasing the BF_4^- basis set size from aug-cc-pvDz to aug-cc-pvTz resulted in changes of the Li^+/BF_4^- complex energy of <1 kcal/mol. The B3PW91 density functional yielded the best agreement with the MP2(full correlations) calculations for the aug-cc-pvDz (B,F) and [5s3p2d] (Li) and is used for studies of the Li^+/BF_4^- complex. The B3PW91 complex energies also showed the best agreement with the MP2 calculations in the previous studies of Li^+/PF_6^- complexation.[20] The Li^+/BF_4^- complex energies (Table 1) were calculated at

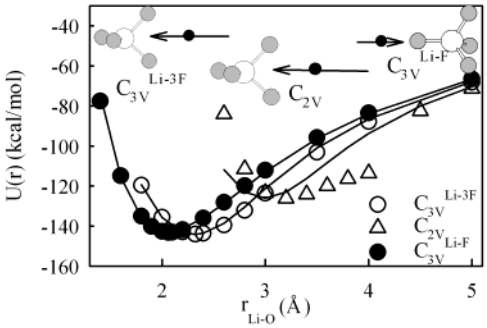

Figure 1. Total binding energy from the B3PW91/aug-cc-pvDz, [5s3p2d] levels (symbols) and from molecular mechanics calculations using the developed force field (solid lines) along the C_{3v}^{Li-3F}, C_{2v}, and C_{3v}^{Li-1F} paths. Geometry optimization was performed for each Li−B separation in both the quantum chemistry and molecular mechanics calculations.

TABLE 2: Partial Charges and Polarizabilities of BF_4^-

element	partial charge (e)	polarizability (Å^3)
Li	1.0	0.0
B	1.072	0.0
F	−0.518	0.89

the B3PW91/(aug-cc-pvDz,[5s2p2d]) level for the C_{2v} and C_{3v}^{Li-1F} (the C_{3v} symmetry complex with one Li−F bond) complexes shown in Figure 1. The C_{2v} complex is the most stable, with an energy of −144.0 kcal/mol; the C_{3v}^{Li-3F} complex has a slightly lower stability, with a complex energy of −142.7 kcal/mol, whereas the C_{3v}^{Li-1F} complex was the least stable, with a complex energy of only −126.2 kcal/mol.

We proceed with development of the Li^+/BF_4^- force field. An absence of the valence electrons leads to a very small polarization of Li^+ (0.03 Å^3) at the MP2(full electron correlations)/[5s3p2d] and B3LYP/[5s3p2d] levels, which suggests a negligible dispersion interaction between the Li^+ and BF_4^-, in agreement with the small difference between the HF and MP2-(full) Li^+/BF_4^- complex energies. Therefore, we have set the Li^+ polarization and Li^+/BF_4^- dispersion parameters to zero in the Li^+/BF_4^- force field. The BF_4^- partial charges were determined by fitting the electrostatic grid around BF_4^-, whereas the atomic polarizability of the boron and fluorine atoms was determined by fitting the polarizable energy along the paths shown in Figure 1, in a manner similar to the procedure previously described for PEO.[22] The resulting partial charges and polarizabilities are shown in Table 2. The B−F bond length (1.421 Å), and the F−B−F equilibrium bending angle (109.47°), were obtained from the fit to the BF_4^- equilibrium geometry, whereas the bending force constant (150 kcal mol^{-1} rad^{-2}) and B−F force constant (368 kcal mol^{-1} Å^{-2}) were adjusted to reproduce the distortion energy of BF_4^- upon extension and compression of the B−F bond length within 0.2 Å from the equilibrium chemistry and the F−B−F bending angle distortion energy within 10° of the equilibrium at the B3PW91/aug-cc-pvDz level.

The form of the potential function used for the PEO/$LiBF_4$ force fields is described in Section IV of ref 22 (eqs 1−7) and elsewhere.[19,20,22,28] The repulsion parameters (*A* and *B*) for the Li^+/BF_4^- interactions were obtained by fitting the Li^+/BF_4^- complex energies along three paths, as shown in Figure 1, with geometry optimizations performed for each Li−B separation. The resulting repulsion parameters are shown in Table 3. The fits were excellent for the C_{3v}^{Li-3F} and C_{2v} paths, i.e., within 0.5 kcal/mol for the most energetically stable C_{3v}^{Li-3F} and C_{2v} geometries, whereas the force field predicted weaker Li^+/BF_4^- binding along the C_{3v}^{Li-F} path. The reason for the discrepancy between the force field and the quantum chemistry is a much larger Li−B bond extension (up to 0.5 Å), resulting in closer Li−F distances in quantum chemistry calculations, compared to the force field, and a reduction in the Li^+/BF_4^- complex energy. This large B−F extension is not adequately described by the force field. Reducing the B−F force constant by a factor of ∼8 significantly improves the agreement between the complex energies along the C_{3v}^{Li-1F} path between Li−B separations of 3−4 Å but worsens the description for Li−B separations of >4.25 Å, together with the description along the other two paths. We have decided to use a B−F force constant of 368 kcal mol^{-1} Å^{-2}, which yields a good description of the most important paths (C_{3v}^{Li-3F} and C_{2v}) instead of improving the force field description along the C_{3v}^{Li-F} path with the weakest Li^+/BF_4^- binding, compromising the description of the most energetically favorable C_{3v}^{Li-3F} and C_{2v} paths. A similar situation was found in the quantum chemistry studies of Li^+/PF_6^- complexation, where a significant lengthening of the P−F bond was observed for the complex with the C_{4v} symmetry.[20]

TABLE 3: Repulsion (*A*) and Dispersion (*B*, *C*) Parameters, and Ion Diffusion Coefficent (*D*), for the Li^+/BF_4^-, Li^+/PEO, BF_4^+/PEO, and BF_4^+/BF_4^+ Force Fields

atom pair	*A* (kcal mol^{-1})	*B* (Å^{-1})	*C* (kcal mol^{-1} Å^{-6})	*D* (kcal mol^{-1} Å^{-4})
Li−Li	44195[a]	7.277[a]	0.0	0.0
Li−B	1257	2.441	0.0	0.0
Li−F	18636	4.082	0.0	0.0 (50)
Li−O	54403	4.545	0.0	100 (120)
Li−C	3581	2.784	0.0	50 (60)
Li−H	3610.0[b]		0.0	5 (6)
B−B	14976[c]	3.090[c]	1150.0[d]	0
B−F	33702	3.577	487.9	0
B−O	32977	4.323	446.8	0
B−C	41335	2.954	891.5	0
B−H	21690	3.244	177.4	0
F−F	66641[e]	4.301[e]	93.5	0
F−O	19294[f]	3.474	119.0	0
F−C	19294[e]	3.431[e]	237.5	0
F−H	12300[g]	4.143[g]	53.9	0

[a] From ref 19. [b] The A/r^{12} form of the potential was used for the Li−H interaction. [c] Assumed to be similar to C−C, the actual value is not significant, as B−B close separations are highly improbable. [d] Ionization potential and polarizability values for B^+ were used. [e] From fits to the CF_4 dimer at the HF/aug-cc-pvDz level. [f] The *A*(F−O) coefficient was assumed to be similar to the *A*(F−C) parameter. [g] From the PFDV force field reported by Byutner et al. (Byutner, A.; Smith, G. D.; Jaffe, R. L. *Macromolecules* **2000**, *33*, 4264.)

B. Li^+/Ether Complexation Energetics. We begin development of the Li^+/ether force field by establishing the adequate levels of theory for calculation of the Li^+/ether complexation energy, which is defined as the total energy of the complex minus energy of reactants at optimized geometries. Table 4 shows that total complexation energies of −38.1 and −38.5 kcal/mol for Li^+/ether at the MP2(full) level, using aug-cc-pvDz and aug-cc-pvTz basis sets for ether and [5s3p2d] basis set for Li^+, agree nicely with the previously reported accurate G2(MP2,-SVP) value of −37.9 kcal/mol.[29] B3LYP and HF calculations, using the aug-cc-pvDz basis set, predict a slightly higher complexation energy (by 1−1.5 kcal/mol) for the Li^+/ether complex. B3LYP/aug-cc-pvDz level calculations yield better agreement with the MP2/aug-cc-pvTz level calculations than the HF/aug-cc-pvDz level calculations for the nonbonded (or intermolecular) contribution to the complexation energy (U^{N-B}); therefore, we will use the B3LYP/aug-cc-pvDz level for further calculations of U^{N-B}.

The repulsion contribution to the Li^+ complexation energies can be determined from quantum chemistry calculations by subtracting the energy of the (charge 1 e)/molecule complex from the energies of the Li^+/molecule complex at the same geometry. The repulsion energy from the B3LYP/(aug-cc-pvDz for PEO, [5s3p2d] for Li^+) calculations along the four representative paths shown in Figure 1 in ref 22 are presented in Figure 2. The repulsion parameters *A* and *B* were determined by fitting the quantum chemistry repulsion energies and are shown in Table 3. The resulting fits shown in Figure 2 are good, which indicates that the functional form (eq 2 of ref 22) is adequate for reproducing the repulsion of ethylene oxide oligomers and Li^+, whereas the A/r^{12} functional yields a much steeper repulsion than that of the quantum chemistry (not shown).

The nonbonded contribution to the complexation energy in our force field is approximated by the coulombic, many-body polarizability, and repulsion terms. Again, because of an insignificant Li^+ polarizability, Li^+ dispersion parameters for

TABLE 4: Total BSSE-Corrected Complexation Energy (E^{tot}), BSSE-Corrected Nonbonded Part of Complexation Energy ($E^{N-B} = E^{tot} - E^{dist}$), and Distortion Energy (E^{dist}) for Li^+/Ether and Li^+/EO_4 Complexes[a]

level of theory/basis set for geometry optimization	level of theory/basis set for energy calculation	E^{tot} (kcal/mol)	E^{N-B} (kcal/mol)	BSSE (kcal/mol)	E^{dist} (kcal/mol)
		Li^+/ether			
B3LYP/aug-cc-pvDz	B3LYP/aug-cc-pvDz	−39.74	−40.79	0.15	1.05
B3LYP/aug-cc-pvDz	MP2(full)/aug-cc-pvDz	−38.08	−38.91	0.84	0.84
MP2(full)/aug-cc-pvDz	MP2(full)/aug-cc-pvDz	−38.11	−39.05	0.84	0.95
MP2(full)/aug-cc-pvDz	MP2(full)/aug-cc-pvTz	−38.47	−39.87	0.51	1.40
B3LYP/aug-cc-pvDz	HF/aug-cc-pvDz	−39.41	−41.37	0.10	1.96
		Li^+/EO_4			
B3LYP/aug-cc-pvDz	B3LYP/aug-cc-pvDz	−96.7		0.7	
B3LYP/aug-cc-pvDz	MP2(full)/aug-cc-pvDz	−96.5		2.1	9.4
B3LYP/aug-cc-pvDz	HF/aug-cc-pvDz	−94.3		0.5	17.8

[a] The Li basis set [5s2p2d] was used.

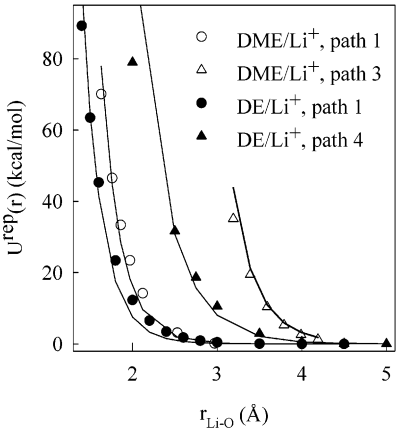

Figure 2. Repulsion contribution to the total binding energy of dimethyl ether (DE) with the Li^+ cation, and of 1,2-dimethoxyethane (DME) with the Li^+ cation, along the paths from Figure 1 in ref 22, from B3LYP/aug-cc-pvDz quantum chemistry calculations, and from the force field.

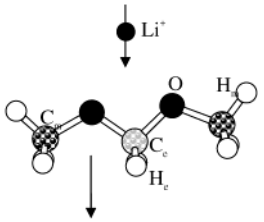

Figure 3. Schematic of the lowest-energy DMM/Li^+ complex. The two paths used for calculation of the atomic polarizabilities are shown with arrows.

interactions with PEO carbon, oxygen, and hydrogen atoms are set to zero. A negligible Li^+ polarizability also indicates that all of the many-body polarization energy comes from Li^+ cations that are polarizing the PEO and almost none from PEO that is polarizing the Li^+ cation. The coulombic contribution to the DME/Li^+ and DE/Li^+ complexation energy is completely determined by the partial charges obtained in the previous manuscript[22] (i.e., the FF-1 and FF-3 force fields) and the Li^+ charge of 1 e. The many-body polarizable contributions to the complexation energy are completely determined by PEO polarizabilities, as described in ref 22.

We test the ability of the PEO force fields FF-1 and FF-3 that are developed in the previous paper[22] and the Li^+/PEO repulsion parameters that have been developed here to predict the quantum chemistry complexation energy for the Li^+/(triglyme = EO_4) complex reported in Table 4. The FF-1 force field predicts a total complexation energy of Li^+/EO_4 of −84.6 kcal/mol, whereas the FF-3 force field yields a higher complexation energy of −91.5 kcal/mol. The FF-1 force field significantly underestimates (by 11.9 kcal/mol) the quantum chemistry complexation energy of the Li^+/EO_4 complex (−96.5 kcal/mol at the MP2/aug-cc-pvDz level); the FF-3 force field does a much better job in predicting the Li^+/EO_4 complex energy, underestimating it by 5 kcal/mol. These results are consistent with the more significant underestimation of the electrostatic potential in the proximity of ether oxygen by the FF-1 force field than by the FF-3 force field shown in Figure 3 in ref 22. The FF-3 force field will be used for the MD simulations of PEO/$LiBF_4$ presented below, because it can describe the PEO/Li^+ interactions more accurately than the FF-1 force field.

C. Transferability of the PEO/Li^+ Force Field to the Other Polyethers. We investigate the transferability of the force field by checking its ability to predict the nonbonded part of the complexation energy of Li^+ cations with dimethoxymethane (DMM), which is an oligomer of poly(oxymethylene) (POM). The geometry optimization of the DMM/Li^+ complex was performed at the B3LYP/(aug-cc-pvDz for DMM, [5s3p2d] for Li^+) level. The most stable DMM/Li^+ complex shown in Figure 3 adopts the high-energy trans−trans (tt) conformation, allowing favorable DMM dipole interaction with the +1 e charge on the Li^+ cation. The nonbonded part of the DMM/Li^+ complex energy, which is defined as the energy of the complex minus the energy of DMM and the Li^+ cation in the complex geometry, was −59.5 kcal/mol, after a BSSE correction of 0.2 kcal/mol. To determine the DMM/Li^+ complex energy from molecular mechanics calculations with the classical force field, one must know the coulombic and many-body polarizable contributions to the complex energy, which are determined by the DMM partial charges and polarizabilities. The partial charges were determined analogously to the PEO charges,[22] yielding the charges shown in Table 5. The hydrogen partial charges are similar between the POM and PEO force fields, as expected, whereas the backbone carbon partial charge (C_e) is more positive in the POM force field, because there are fewer carbon atoms in POM to donate charge to EO atoms in POM than there are in PEO. The atomic polarizabilities of DMM atoms were fit analogously to those in PEO, with the C_m and H polarizabilities being constrained to those of the dimethyl ether (PEO force field). The oxygen and carbon polarizabilities were found to be similar between the POM and PEO force fields, as expected.

The geometry optimization was performed using molecular mechanics with the partial charges and polarizabilities from Table 5 and the repulsion parameters from Table 3. The nonbonded part of the complex energy, computed at the minimum geometry, was −58.2 kcal/mol, which is only 1.3 kcal/mol different from the quantum chemistry value of −59.5 kcal/

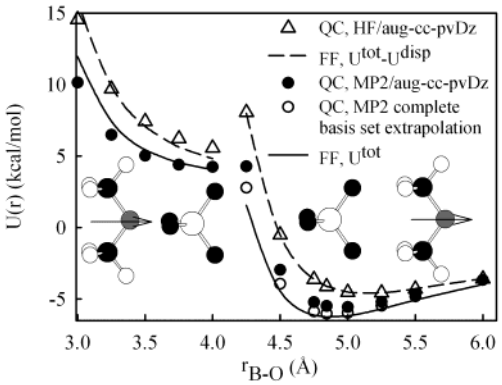

Figure 4. The ($U^{tot} - U^{disp}$) contribution to the total binding energy of dimethyl ether (DE) with the BF_4^- anion from the force field and from the HF/aug-cc-pvDz level quantum chemistry calculations. The total DE/BF_4^- complex energy from the force field and the MP2/aug-cc-pvDz level, and the MP2/complete basis set extrapolation, are also shown.

TABLE 5: Charges and Polarizabilities for the Poly(oxymethane) (POM) Force Field Obtained by Fitting an Electrostatic Grid around Dimethoxymethane (DMM)[a]

atom type	polarizability (Å^3)	charge (e)
C_m	1.672 (1.672)	−0.0322 (−0.1187)
C_e	1.52 (1.395)	0.2470 (−0.0326)
O	0.95 (1.129)	−0.3526 (−0.2792)
H_e	0.176 (0.176)	0.0528 (0.0861)
H_m	0.176 (0.176)	0.0695 (0.0861)

[a] Parameters for the PEO force field are shown in parentheses.

mol. This accuracy of ∼1 kcal/mol is similar to the accuracy of the quantum chemistry calculations at the B3LYP/(aug-cc-pvDz for DMM, [5s3p2d] for Li^+) level, which indicates the ability of the developed PEO/Li^+ force field to predict the complex energies of the oligomers of POM with Li^+ cations. Therefore, we conclude that the repulsion parameters of the PEO/Li^+ force field are transferable to other polyether/Li^+ complexes. Moreover, the similarity between the DMM and DME polarizabilities indicates that the polarizabilities could also be considered transferable in the first approximation.

D. Dimethyl Ether/BF_4^- Complex. The repulsion contribution to the DE/BF_4^- complex energy was obtained from the HF/aug-cc-pvDz and HF/aug-cc-pvTz calculations for two geometries, as shown in Figure 4. The BSSE correction was applied in the calculation of all energies. The HF/aug-cc-pvDz energies were within 0.1 kcal/mol of the HF/aug-cc-pvTz energies, with an average deviation of 0.03 kcal/mol along the lower-energy path, indicating that aug-cc-pvDz is an adequate basis set for description of the repulsion contribution in the DE/BF_4^- complex energy. As seen for a dimethyl ether/dimethyl ether complex,[22] much larger basis sets are required for prediction of the correlation energy (dispersion contribution). The BSSE-corrected correlation energy (MP2 − HF) for the MP2/aug-cc-pvDz was found to be 22%−36% smaller than that determined at the MP2/aug-cc-pvTz level, which indicates that the MP2/aug-cc-pvDz level significantly underestimates the dispersion contribution. An extrapolation to the complete basis set limit was performed, assuming that the X^{-3} scaling of the correlation energy with the basis set size. The correlation energy at the complete basis set limit is 30%−50% higher than that for the MP2/aug-cc-pvDz level, depending on the BF_4^-/DE separation. We used an average scaling factor of 1.4 to scale all the BSSE-corrected MP2/aug-cc-pvDz values to the complete basis set limit for the lowest energy path, as shown in Figure 4. The repulsion parameters for the DE/BF_4^- interaction were determined by fitting the BSSE-corrected HF/aug-cc-pvDz energies along the two paths shown in Figure 4, unless indicated otherwise in Table 2.

Calculation of the correlation energy that is required for determination of the dispersion parameters is computationally expensive; therefore, we have adopted a different strategy for calculation of the dispersion parameters. First, we use the London dispersion formula given by eq 1 to obtain the first approximation of the dispersion parameters, and then we use the complete basis set extrapolation to check the agreement between these parameters and correlation energy from quantum chemistry:

$$C_{\alpha\beta} = -\frac{3}{2}\left(\frac{IP_\alpha IP_\beta}{IP_\alpha + IP_\beta}\right)\alpha_\alpha\alpha_\beta \qquad (1)$$

where IP_α and IP_β are the respective ionization potentials for atom types α and β, and α_α and α_β are the polarizabilities of atom types α and β. The following parameter values were used: $\alpha_C = 1.76$ Å^3, $\alpha_O = 0.802$ Å^3, $\alpha_H = 0.667$ Å^3, $\alpha_F = 0.557$ Å^3, $\alpha_B = 3.030$ Å^3, $IP_C = 259.67$ kcal/mol, $IP_O = 314.04$ kcal/mol, $IP_H = 313.58$ kcal/mol, $IP_F = 401.78$ kcal/mol, and $IP_B = 191.36$ kcal/mol.[30] The dispersion energy from the London formula approximation compares well with the complete basis set extrapolation of the BSSE-corrected MP2 energies along the lower energy path, which indicates that the dispersion parameters from the London approximation are similar to the quantum chemistry parameters and could be used in MD simulations without further modification. Complete basis set extrapolations were not performed for the higher-energy path; however, if the same scaling factor as that used for the lower-energy path (1.4) is used for the higher-energy path to obtain the complete basis set limit, one would need to increase the F−O dispersion parameters by ∼40%−50% from those obtained by the London formula to match the quantum chemistry data. We note that the complex energies along the lower-energy path are relatively insensitive to the F−O interaction, because of large F−O separations.

E. Two-Body (TB) Force Field for PEO/$LiBF_4$. Because MD simulations with the many-body polarizable terms are ∼2−4 times more expensive, in comparison to the MD simulations of identical systems with a force field containing only two-body interactions, it is desirable to develop a TB force field for PEO/$LiBF_4$ interactions that considers the many-body polarizable effects in a "mean-field" sense. Considering only the lowest-order term in r_{ij} in eqs 3 and 4 in ref 22, the polarization energy between two charged atomic centers with dipolar polarizability is given by eq 2:

$$U^{POL}(r_{ij}) = -332.07\left(\frac{q_i^2\alpha_j + q_j^2\alpha_i}{2r_{ij}^4}\right) = -\frac{D_{ij}}{r_{ij}^4} \qquad (2)$$

where α_i are α_j the atomic dipole polarizabilities. This expression for U^{POL} is exact only for systems with two ions. For systems with more than two charged polarizable atoms, eq 2 is not exact, because it neglects interactions between the induced moments. However, the induced dipole−induced dipole interactions are usually much less than the permanent charge-induced dipole moment interactions, which indicates that eq 2 might be a good approximation.

In our previous work on PEO/LiI[19] and PEO/$LiPF_6$,[20] we included the effective two-body polarization terms in the force field. We used *D*-parameters obtained from the fits to the ab

initio quantum chemistry calculations of the Li/ether energies that were uniformly scaled by a factor of 0.71, to account for the condensed-phase effects. This factor of 0.71 was obtained from a detailed investigation of the incremental $Li^+/(ether)_n$ complex energies (for $n = 1, 2, 3, 4$). It was found that the polarization energy of $Li^+/(ether)_4$, representing the Li^+ coordination in a condensed phase, is described well by two-body polarization terms (eq 2) parametrized for the Li^+/single-ether complex and is scaled by a factor of 0.71 to obtain good agreement with quantum chemistry energies for the $Li^+/(ether)_4$ complex. In this work, we take a different and more rigorous approach for obtaining *D*-parameters. In particular, we perform MD simulations of PEO/$LiBF_4$ solutions at an EO:Li concentration of 15:1 at 393 K, using the MB polarizable force field described below. The induced dipole moments and charges from these simulations will be used to estimate the polarizable energy between the induced dipole moment and the Li^+ cation, as a function of separation, allowing us to estimate the *D*-parameters from eq 2. The D_{ij} parameters were found to be dependent on the distance between atoms *i* and *j*; thus, the D_{ij} parameter at the first peak of the radial distribution function between atoms *i* and *j* are used. Following our previous work, the D_{ij} parameters are scaled to zero beyond the first coordination shell of Li^+ (3.5 Å), using a distance-dependent dielectric constant, because the PEO and BF_4^- molecules outside the Li^+ coordination shell are likely to be located in the first coordination shell of the other Li^+ cations and are likely to be strongly polarized by them.

The initial MD simulations of the PEO/$LiBF_4$ solutions (EO:Li = 15:1) at 393 K with the two-body potential parametrized as previously described indicated that these simulations yield ion dynamics that are slower and a lower fraction of the Li^+ cations that are not complexed by the BF_4^- cations than those from the MD simulations with the MB polarizable force field. We subsequently set the D^{Li-F} parameters to zero and decreased the other *D*-parameters by ~20%, to decrease the strength of interaction between Li^+ with PEO and BF_4^-, thus increasing the ion dynamics and improving the agreement for the fractions of "free" Li^+ cations from MD simulations with the MB and TB potentials within the simulation error.

IV. Molecular Dynamics Simulations of PEO/$LiBF_4$ Solutions

A. Molecular Dynamics Simulation Methodology. MD simulations were performed on the PEO (M_w = 2380)/$LiBF_4$ solutions for the ratio of ether oxygen (EO) to Li of 15:1 (EO:Li = 15:1) at temperatures of 423, 393, and 363 K, using the many-body polarizable (MB) and two-body force field with the effective two-body polarizability (TB). The simulation box consisted of 10 PEO chains and 36 anions and cations. A Nose−Hoover thermostat[31] and a barostat[32] were used to control the temperature and the pressure, whereas the bond lengths were constrained using the Shake algorithm.[33] The Ewald summation method was used for treatment of the long-range electrostatic forces between partial charges with partial charges and partial charges with induced dipoles for the many-body polarizable potential, and the particle−mesh Ewald (PME) technique[34] was used for the simulations that used the two-body nonpolarizable potential. A tapering function[35] was used to drive the induced dipole−induced dipole interactions to zero at the cutoff of 10 Å. A multiple-time-step reversible reference system propagator algorithm was employed,[36] with a time step of 0.75 fs for bonding, bending, and torsional motions, a 1.5 fs time step for nonbonded interactions within a 6.5 Å sphere and a 3.0 fs time step for nonbonded interactions between 6.5 and 10.0 Å and the reciprocal space part of the Ewald and PME summation. A distance-dependent dielectric constant was used for scaling of the effective two-body contribution only in the TB force field; the dielectric constant was unity for atom separations of <3.5 Å, and then scaled from unity at 3.5 Å to the value of 100 at the cutoff radius.

B. Characteristic Time Scales for Dynamics in Polymer Electrolytes. The dynamics of polymer electrolytes are complex, because of the presence of many characteristic time scales that are dependent on the polymer molecular weight, nature, and concentration of salt, temperature, and barriers of polymer conformational transitions. For example, in our PEO (M_w = 2380)/$LiBF_4$ (EO:Li = 15:1, 393 K), the torsional transitions occur on the time scale of $\sim 10^{-11}-10^{-10}$ s, characterizing local polymer dynamics, whereas $\sim 10^{-7}$ s are required for PEO to diffuse a distance equal to its own size, i.e., a radius of gyration (~14 Å). The characteristic time scale for the Li^+ cation and the BF_4^- anion to diffuse a distance equal to the radius of gyration of a PEO chain is on the order of tens of nanoseconds ($\sim 10^{-8}-10^{-7}$ s). The ion−cation residence time and the ion−EO residence times are on the order of 10^{-8} s. Analysis of these time scales indicates that the system must be equilibrated for a long time (for MD simulations), i.e., 10^{-7} s, for PEO to reach equilibrium global conformations, for ions to diffuse a distance on the order of the PEO chain length, and for every cation to associate and dissociate with any anion at least once, on average.

C. Initial Configurations of PEO/$LiBF_4$ Systems. How Long Does It Take for Polymer Electrolyte Systems to Equilibrate? Long equilibration time scales pose challenges for obtaining equilibrium structural and dynamic properties. This issue has not been adequately considered in the previous MD simulations of polymer electrolytes,[11−14] probably because of the lack of computational time required for the investigation of system equilibration. In this contribution, we explore the time scales for a polymer electrolyte equilibration by creating three systems of PEO (M_w = 2380)/$LiBF_4$ (EO:Li = 15:1, 393 K) with their initial configurations corresponding to different ion aggregation states: *system 1* has the majority of ions (>80%) being a part of ion aggregates or ion pairs; *system 2* has the majority of ions (>80%) existing as free ions (i.e., ions that do not have any counterions in their first coordination shell of 4 Å) and essentially no ion aggregates; and *system 3* is in the intermediate aggregation state with ~30% free Li^+ cations, 10% free BF_4^- anions, and significant ion aggregation. It is expected that the equilibrium state of ion aggregation will be somewhere between those for the initial configuration of systems 1 and 2, which allows us to estimate lower and upper boundaries for the structural and dynamic properties.

We begin the investigation of equilibration time scales using the TB force fields (FFs), because they are computationally 3−4 times less expensive. After 5-ns NPT runs for each system of PEO (M_w = 2380)/$LiBF_4$ (EO:Li = 15:1, 393 K), we changed the box size to that corresponding to 1 atm of pressure and started 100-, 80-, and 70-ns NVT runs for systems 1, 2, and 3, respectively, which were created as previously described. Monitoring of the fraction of free cations and anions, as shown in Figure 5a,b, allows us to gauge changes in ion aggregation with time for each system. Figure 5a demonstrates that the fraction of free ions in the first system dramatically increases over the first 10 ns, showing only a gradual increase over the next 90 ns, to 50%−60%, whereas the second system has the number of free Li^+ cations fluctuating in the range of 65%−80%. The third (intermediate) system showed an intermediate behavior. Monitoring of the number of free BF_4^- anions versus

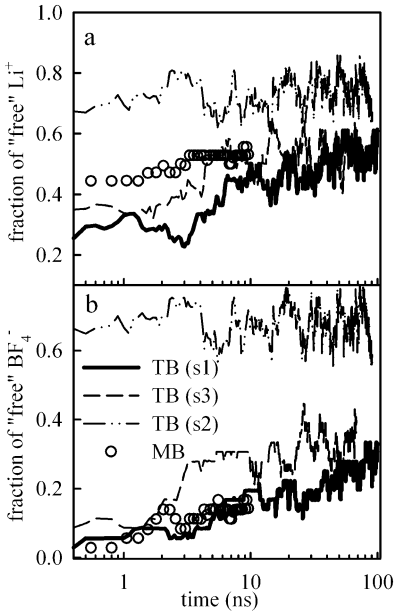

Figure 5. Fraction of (a) "free" Li^+ cations and (b) "free" BF_4^- anions during the simulation run for PEO/$LiBF_4$ (EO:Li = 15:1, 393 K) for MB and TB force fields. Pre-equilibration runs of 4 ns for MD simulations with the MB force field and 15 ns for those with TB force fields were omitted.

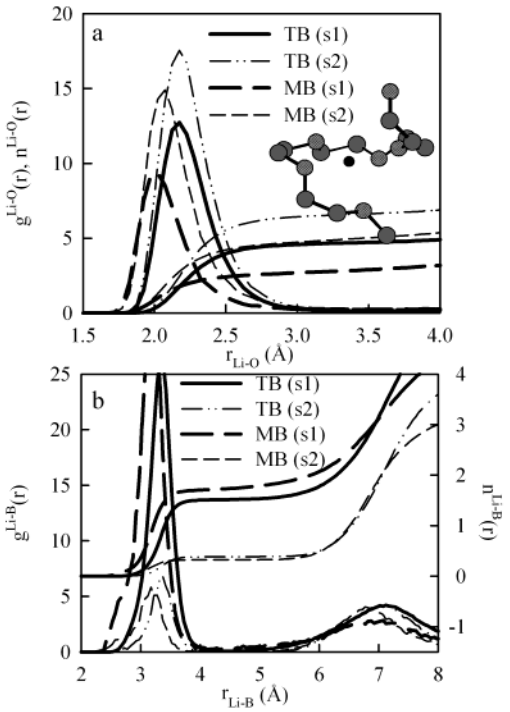

Figure 6. Radial distribution functions (RDFs) ((a) for Li−O and (b) Li−B interactions) and coordination numbers for PEO/$LiBF_4$ (EO:Li = 15:1, 393 K). Typical Li^+ coordination by a PEO segment is also shown.

time showed a tendency that was similar to that observed for the behavior of free Li^+ cations. It is interesting that, even after 100-ns and 80-ns runs for systems 1 and 2, respectively, the numbers of free cations and free anions are still different between the systems—by 20% and 40%, respectively—which indicates that present simulations allow us to obtain fractions of free ions with accuracies of 20% and 40% for free cations and anions. The use of parallel tempering algorithms is a promising route for the acceleration of system equilibration[37] and is recommended for future equilibration of polymer electrolytes. The differences in ion aggregation shown in Figure 5 are likely to result in some differences in ion environment and ion transport. Therefore, we perform analysis of the structural and dynamic properties for both systems 1 and 2, to estimate the effect of initial conditions and ion aggregation on cation environment, ion self-diffusion coefficient, and conductivity. System 3 showed intermediate behavior and will not be discussed below.

MD simulations with the MB force field were performed on the PEO/$LiBF_4$ system created from system 1 after 5 ns of equilibration. This system showed the time dependence of the fraction of free cations and anions, similar to that for the TB force field, as seen from Figure 5. We also created a second system for simulations with the many-body polarizable interactions. The initial configuration of the second system was taken after 30 ns of simulations with the TB force field of system 2. This system was simulated for 1 ns.

The temperature dependence of the structural and dynamic properties of the polymer electrolyte was investigated by performing simulations at 363 and 423 K for both TB and MB force fields. Only system 1, i.e., the aggregated system, was investigated at 363 and 423 K. Initial configurations were taken from the configuration after 50 ns of MD simulations of system 1 at 393 K. MD simulations at 363 and 423 K were performed for 9 ns for the MB force field and for 50 ns for the TB force fields.

D. Structural Properties of PEO/$LiBF_4$. The structure of the Li^+ environment is of great interest, because it is expected to be intimately related to the Li^+ transport mechanism. The last 5 ns of simulations employing the TB force field and the last 0.5 ns of simulations employing the MB force field were included in the analysis of the structural properties. We begin analysis of the Li^+ environment by calculating the radial distribution functions (RDFs, $g^{Li-X}(r)$) and distance-dependent coordination numbers ($n^{Li-X}(r)$), shown in Figure 6, for the MD simulations with the MB and TB force fields for systems 1 and 2. The position of the first peak of the Li−O RDF is ∼2.02−2.05 Å for the MB force fields and 2.15−2.20 Å for the TB force fields. These most probable distances from MD simulations are similar to the Li−O most probable distance of 2.07−2.1 Å that was obtained from analysis of the NDIS experiments on PEO/LiI[4,5] and PEO/LiTFSI,[38] indicating that both force fields (MB and TB) reasonably reproduce the structure of the Li^+−PEO complexation. The Li−O RDFs for system 2 are systematically higher than those for system 1, because system 2 has a higher fraction of free cations than system 2, allowing more EO atoms to enter the first coordination shell of the Li^+ cation, as seen from $n^{Li-O}(r)$ and also presented in Figure 6a. We define EO atoms as being complexed by a Li^+ cation if they are within 3 Å of a Li^+ cation. Figure 6a demonstrates that the number of EO atoms complexed by a Li^+ cation varies significantly (in the range of 2.7−6.4), depending on the type of force field and the state of system aggregation. The number of complexed EO atoms is higher, by ∼2 EO atoms, for system 1 than for system 2 for both force fields, which indicates that, despite our long MD simulations, we can predict the average number of complexed EO atoms within an accuracy of 2 EO atoms, depending on the initial configuration that we choose. The MB force fields predict ∼2 fewer EO atoms in the first coordination shell of a Li^+ cation than the MB force fields, because of shorter Li−O distances for the MB force field, resulting in a more compact first coordination shell.

Analysis of the Li−B RDF and coordination number shown in Figure 6b indicates a strong preference of an anion to be in

the first coordination shell of a Li^+ cation for system 1 (the system with the larger fraction of ion aggregates) and a much weaker Li−B affinity for system 2. Coordination numbers of 1.7 (MB system 1) and 0.3 (MB system 2) boron atoms and 1.5 (TB system 1) and 0.4 (TB system 2) boron atoms of BF_4^- anions within a 4-Å coordination sphere of a Li^+ cation were found, on average. The TB and MB force fields yield a very similar number of BF_4^- anions in the first coordination shell of a Li^+ cation, whereas a greater number of anions was observed for the system that started in the aggregated state (system 1), compared to the system that started with the majority of ions dissociated (system 2), again demonstrating the dependence of property on the initial conditions.

To analyze the nature of cation−anion complexation in greater detail, the probabilities of finding a certain number *n* of BF_4^- anions in the first coordination shell of a Li^+ cation forming the $Li^+-BF_4^-{}_n$ complexes and the probability of finding a certain number *m* of Li^+ cations in the first coordination shell of a BF_4^- forming the $BF_4^--Li^+{}_m$ complexes were calculated and are shown in Figure 7a,b. All the systems predict that the Li^+ cations prefer to either exist as free lithium or be coordinated by four BF_4^- anions. No preferential coordination of the BF_4^- anions by Li^+ cations is observed. Instead, the BF_4^- anions show a broad distribution of the number of Li^+ cations in its first coordination shell. The probability of finding a certain number *n* of EO atoms in the first coordination shell of a Li^+ cation is shown in Figure 7c. This figure indicates that the MB force field predicts a Li^+ coordination of five EO atoms to be the most probable, whereas a coordination of seven EO atoms wrapped around the Li^+ cation is the most probable for the TB force field. The most probable number of EO atoms around the Li^+ cation—5 (MB) and 7 (TB)—is the same for systems 1 and 2 and, therefore, is considered to be independent of the initial configuration.

The Li^+ complexation was also found to perturb the PEO local and global conformations significantly, resulting in an increase of the fraction of the tgt and tgg conformers of −O−C−C−O− sequences and a decrease in the fraction of ttt, tg^+g^-, and ttg dihedrals. The PEO radius of gyration decreased as $LiBF_4$ was added, because the Li^+ cation is typically wrapped by a PEO segment, as shown in Figure 6. These structural changes are in accord with the experimental data and are independent of the choice of the force field (i.e., MB or TB) or initial configuration of the system. Similar findings were reported for our previous PEO/LiI simulations[4] and PEO/Li−triflate simulations[17] and, therefore, are not discussed here.

E. Effect of the Li^+ Cation on Poly(ethylene oxide) Dynamics. Quasi-elastic neutron scattering (QNS) experiments have shown that the addition of salts slows the polymer dynamics.[14] ^{13}C spin-lattice relaxation NMR experiments also probe the polymer dynamics, as discussed in ref 22. We have performed the ^{13}C spin-lattice NMR experiments on PEO (M_w = 1854) that was obtained from Sigma−Aldrich, with $LiBF_4$ salt (EO:Li = 15:1) and without salt, at 393 K, for comparison with the simulation results. A ratio of T_1(pure PEO)/T_1(PEO/$LiBF_4$) of 2.9 (where T_1 is the spin-lattice relaxation time) was found in the NMR experiments that were performed according to the previously described methodology.[23] The T_1 spin-lattice relaxation times were also calculated from the MD simulations, as described in Section V.E. of ref 23. The decay from 1 to 0.005 of the P_2^{CH} C−H vector autocorrelation function (ACF) for the interior carbon atoms (see section V.E. of ref 23 for definition) was fitted with the MKWW function and used in eqs 8 and 9 in Section V.E. of ref 23 to calculate the spectral

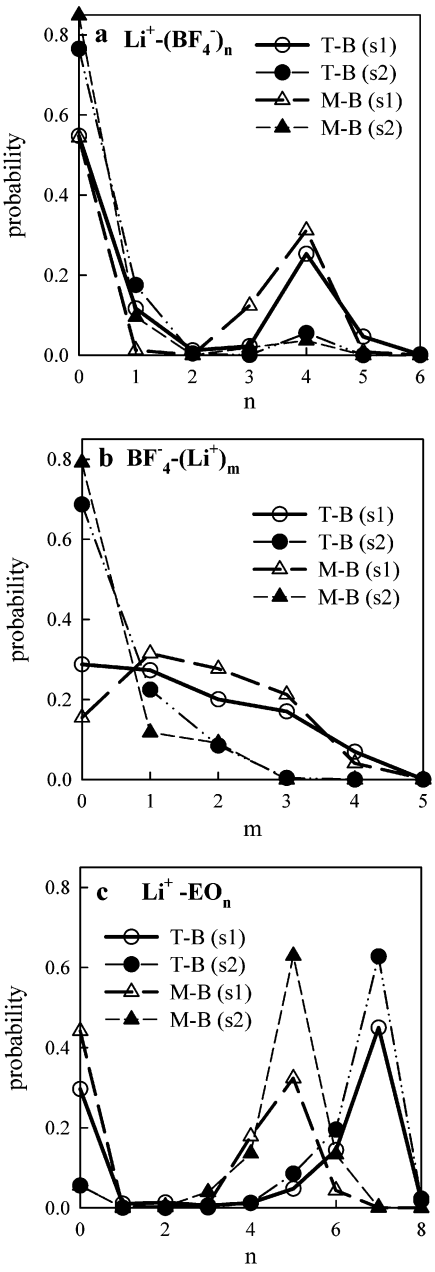

Figure 7. Probability of the (a) $Li^+-(BF_4^-)_n$, (b) $BF_4^--Li^+{}_m$, and (c) Li^+-EO_n coordinations.

density and the T_1 spin−lattice relaxation times. The T_1(pure PEO)/T_1(PEO/$LiBF_4$) ratios calculated from MD simulations are 2.8 for MB system 1, 3.2 for TB system 1, and 4.0 for TB system 2. The T_1(pure PEO)/T_1(PEO/$LiBF_4$) ratio from MD simulations with the MB force field gives the best agreement with experiments, whereas the TB force field predicts a T_1(pure PEO)/T_1(PEO/$LiBF_4$) ratio that is higher than the experimental ratio, which indicates that the TB force field predicts a greater extent of slowing of the PEO dynamics, because of the addition of salt, than that observed in the experiments. These results are consistent with the higher Li^+ coordination number of EO atoms from the TB force field, compared to that from the MB force field, because a greater number of EO atoms from the TB force field makes Li^+ motion along the PEO chain slower, compared to that for the MB force field, as discussed below.

F. Transport Properties of PEO/$LiBF_4$. Ion transport properties, such as the cation and anion self-diffusion coefficient and conductivity, are the most important technologically. Ion self-diffusion coefficients were calculated from MD simulations

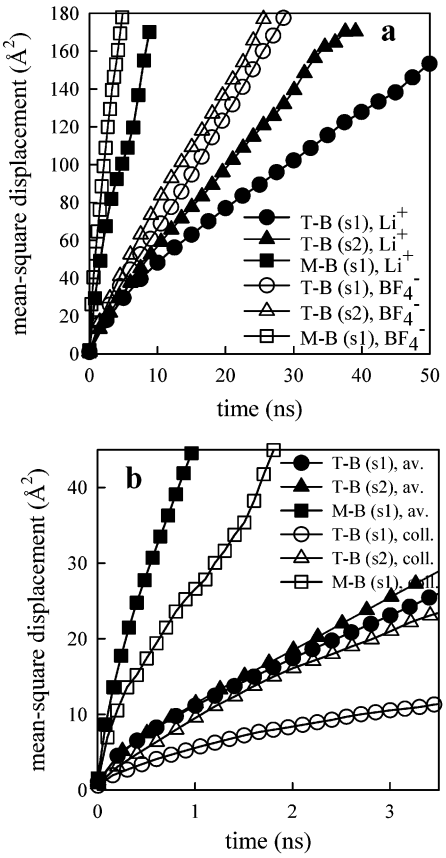

Figure 8. (a) Mean-square displacement of the Li^+ and BF_4^- ions and (b) the average ion displacement and collective ion displacements.

as a slope of mean-squared displacements versus time divided by 6. The conductivity (λ) was calculated using Einstein relation[11]

$$\lambda = \lim_{t\to\infty} \frac{e^2}{6tVk_BTN} \sum_{i,j}^{N} z_i z_j \langle [\boldsymbol{R}_i(t) - \boldsymbol{R}_i(0)][\boldsymbol{R}_j(t) - \boldsymbol{R}_j(0)] \rangle \quad (3)$$

where e is the electron charge, V is the volume of the simulation box, k_B is the Boltzmann's constant, T is the temperature, t is time, z_i and z_j are the charges over ions i and j (given in electrons), $\boldsymbol{R}_i(t)$ is the displacement of ion i during time t, the summation is performed over all ions, the angled brackets ($\langle\rangle$) denote the ensemble average, and N is the total number of ions in the simulation box. The collective ion diffusion coefficient, which represents the mean-square displacement of the charge, is given by eq 4:

$$D_{\text{coll}} = \lim_{t\to\infty} \frac{1}{6tN} \sum_{i,j}^{N} z_i z_j \langle [\boldsymbol{R}_i(t) - \boldsymbol{R}_i(0)][\boldsymbol{R}_j(t) - \boldsymbol{R}_j(0)] \rangle \quad (4)$$

Analysis of the EO and BF_4^- coordination numbers around the Li^+ cation presented in Figures 6 and 7 showed differences in the Li^+ environment between the MB and TB force fields, as well as the dependence of the Li^+ environment on the initial configuration of the system. These differences between the systems are expected to translate into the differences in ion transport properties for the TB and MB systems and systems 1 and 2. Figure 8a presents the Li^+ and BF_4^- mean-square displacement from MD simulations employing the MB and TB force fields for systems 1 and 2. The BF_4^- mean-square displacements for the TB force field is very similar for systems 1 and 2, whereas the Li^+ mean-square displacements indicate that the Li^+ motion in system 1 is slower than that for system 2, probably because of the slower Li^+ motion in ion aggregates, compared to that of free Li^+ cations. Much faster cation and anion motion is observed in MD simulations with the MB force field, compared to that observed with the TB force field.

TABLE 6: Ion Self-Diffusion Coefficients (D) and Conductivities (λ) for PEO/$LiBF_4$ (EO:Li = 15:1, 393 K), Using MB and TB Force Fields, for Systems 1 and 2

system	trajectory length used for analysis (ns)	$D(Li^+)$ (10^{-11} m^2/s)	$D(BF_4^-)$ (10^{-11} m^2/s)	λ (10^{-3} S/m)
system 1, TB	70	0.44	0.98	0.33
system 2, TB	40	0.71	1.11	0.67
system 1, MB	8	4.1	8.3	3.1
system 2, MB	0.8	3.3	7.6	

Next, we investigate the extent of ion correlations by comparing the ratio of the average ion displacements to the collective charge displacements. The average ion diffusion coefficient, $D_{\text{av}} = 0.5[D(Li^+) + D(BF_4^-)]$, is equal to the collective ion diffusion coefficent (D_{coll}) if no ion correlations are present in the system, resulting in the off-diagonal terms in eq 4 adding up to zero. Thus, the deviation of the average ion displacements from the collective charge displacements can serve as a measure of ion correlations in the system. Figure 8b compares D_{av} and D_{coll}. System 1, with a high fraction of ion aggregates, shows significantly slower collective charge displacements than the average ion displacements, because of the large ion correlations in ion aggregates. In system 2 (which consists primarily of free ions), correlations are much less important, resulting in the collective charge displacements being only slightly less than the average ion displacements.

Table 6 summarizes the ion self-diffusion coefficients for the MB and TB force fields for systems 1 and 2. Ion diffusion coefficients from the MB force field are 6−10 times greater than those for the TB force field, which indicates that our two-body approximation, while being able to capture structural properties rather well, predicts significantly slower dynamics. The dependence of the ion transport properties on the initial conditions of the system (aggregated versus free ions) is <50%, which is much less than the difference in ion transport properties between the TB and MB force fields. Because of the relatively small difference in ion transport properties between systems 1 and 2, we have performed an investigation of the temperature dependence of the ion transport properties and studied the mechanism of ion transport only for system 1.

The ion self-diffusion coefficients from MD simulations, as a function of temperature, are compared in Figure 9 with those from the NMR pulse-field-gradient (PFG)[39] measurements of high-molecular-weight oxymethylene-linked PEO ($M_w = 10^5$)/$LiPF_6$, because the ion self-diffusion coefficients are expected to be similar for PEO/$LiBF_4$ and PEO/$LiPF_6$ and no experimental data are available for PEO/$LiBF_4$. The cation self-diffusion coefficient is known to be dependent on the PEO molecular weight;[40] therefore, we used a factor of 1.3, on the basis of experimental investigation of the Li^+ self-diffusion coefficient of PEO molecular weight, to account for the difference between the Li^+ diffusion in PEO ($M_w = 10^5$) and PEO ($M_w = 2380$). The scaled Li^+ self-diffusion coefficients from NMR measurements are ∼2−3 times less than those from MD simulations with the MB force field and are ∼3 times higher than that from the MD simulations with the TB force field. A similar quality agreement between the simulation and the experiments[41,42] is observed for the anion. The conductivities from MD simulations with the MB force field are in better

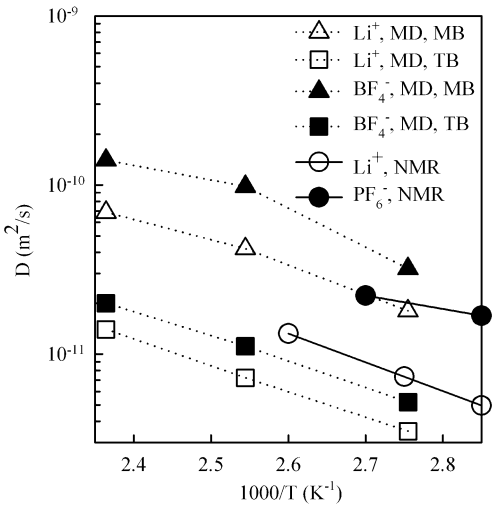

Figure 9. Self-diffusion coefficients of Li^+ and BF_4^- (from MD simulations) and of Li^+ and PF_6^- (from NMR measurements[39]). The scaling factor of 1.5 is based on the molecular weight dependence of Li in PEO/$LiCF_3SO_3$ (EO:Li = 20:1, 90 °C), as measured by NMR.[40]

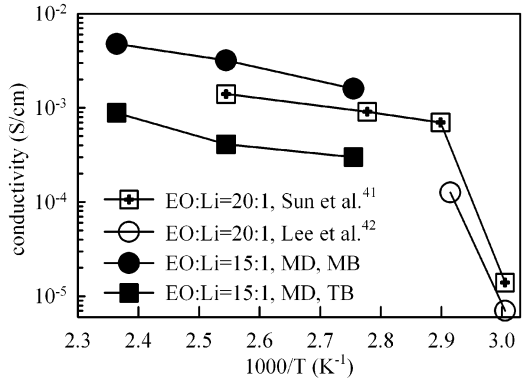

Figure 10. Conductivity from MD simulations and measurements by Sun et al.[41] and Lee et al.[42] (experimental data were corrected for molecular weight differences with MD data).

agreement with the scaled experimental data than those for the TB force field, as shown in Figure 10.

G. Li^+ Transport Mechanism. Having validated the ability of the force fields to represent the structural and dynamic properties of the PEO/$LiBF_4$ polymer electrolytes reasonably, we are in a position to address the controversial issue of the Li^+ transport mechanism in polymer electrolytes. The possible cation transport mechanisms might include Li^+ motion along PEO chains, Li^+ hopping from one PEO chain to the other, Li^+ diffusion with the PEO chain (if the molecular weight of the PEO is below the entanglement molecular weight), and Li^+ diffusion within ion aggregates. Extensive MD simulations of PEO/LiI[12] indicated that all these mechanisms are present. In our MD simulations, we also observe all these mechanisms of Li^+ diffusion. Naturally, the question arises: what is the dominant mechanism(s) of Li^+ diffusion?

Following Müller-Plathe and van Gunsteren,[12] we begin our investigation of the Li^+ transport mechanism by monitoring changes in the Li^+ environment with time. If a Li^+ cation has an EO atom or BF_4^- molecule within 4 Å for 20 ps continuously, a filled circle that is associated with the EO or BF_4^- index number is marked in Figure 11 for that time. The PEO segments of continuous EO atoms are separated by dotted lines in the figure, whereas the blocks with the BF_4^- anions are separated from the EO atoms by the solid lines. Figure 11 shows the representative Li^+ motion types: the $Li^+(1)$, $Li^+(2)$, and $Li^+(4)$ cations are complexed primarily by one segment of consecutive EO atoms, typical for >90% of the Li^+ cations. $Li^+(1)$ and $Li^+(2)$ represent Li^+ cations that do not undergo any significant motion along the PEO chain and, therefore, are moving only with the PEO chains, whereas $Li^+(4)$ represents the Li^+ cations that are moving along the PEO chain and are not being complexed by the BF_4^- anions during the MD simulations; $Li^+(3)$ represents Li^+ cations that are undergoing association−dissociation with different PEO chains and the BF_4^- anions, and $Li^+(5)$ represents Li^+ cations that are moving primarily along the PEO chain, with occasional associations with BF_4^- anions. Figure 11 also shows individual mean-squared displacements for the same five Li^+ cations ($Li^+(1-5)$). The $Li^+(1)$ and $Li^+(2)$ cations, which do not move along the chain, have mean-squared displacements that are significantly below the average, whereas the $Li^+(3)$ and $Li^+(4)$ cations, which undergo significant displacements along the chain or interchain hopping, have mean-squared displacements that are significantly higher than the average. Similar behavior is observed for the other Li^+ cations that are not shown in Figure 11, as well as for the Li^+ cations in MD simulations with the TB force field. We have found that the Li^+ self-diffusion coefficient of Li^+ cations moving along the PEO chain is ∼5 times (MB) and 2−3 times (TB) faster than the Li^+ self-diffusion coefficient of Li^+ cations that are undergoing insignificant movement along a PEO chain, which allows us to conclude that Li^+ motion along the PEO chains makes a very important contribution to the Li^+ transport in PEO/$LiBF_4$.

From the analysis of Li^+ environments versus time, as shown in Figure 11, we have estimated the rate of Li^+ interchain hopping to be $\sim(140\ \text{ns})^{-1}$ per ion and $\sim(500\ \text{ns})^{-1}$ for the MD simulations with the MB and TB force fields, respectively. The rates of Li^+ interchain hopping have large uncertainties, possibly more than 100%, because only a few events occurred during our relatively short simulations and longer simulations are required to get a better estimate. Nevertheless, we proceed with our best estimates and check if they are consistent with the picture of PEO moving along the chain and undergoing interchain hopping. During the mean residence time, which is calculated as the inverse of the rate of Li^+ interchain hopping, a Li^+ cation is expected to travel ∼40−50 Å, which is more than the PEO radius of gyration (∼14 Å) but less than the average end-to-end distance (∼6 × 14 Å = 84 Å), indicating that a Li^+ cation travels a significant distance along the PEO chain before undergoing an interchain jump. In our simulations, we also observe the Li^+ cation leaving the ion aggregates and complexing PEO chains, which suggests an alternative to the interchain hopping mechanism. However, at this point, we cannot estimate the relative importance of interchain hopping versus PEO−aggregate hopping.

Because Li^+ motion along the PEO chains is important, we proceed with estimation of the rate of this motion through estimation of the mean Li^+−EO residence time correlation functions, which are defined by eqs 5 and 6:

$$R_1(t) = \langle H(t)H(0)\rangle \tag{5}$$

$$R_2(t) = \langle \text{average time until EO exits the } Li^+ \text{ coordination shell}\rangle \tag{6}$$

where $H(t) = 1$ if the EO atom is in the first coordination shell of the Li^+ cation and $H(t) = 0$ otherwise. The radius of the coordination shell was set to 3.5 Å. The difference between the residence time correlation functions $R_1(t)$ and $R_2(t)$ is that the $R_2(t)$ function probes the time that the EO atom spends in

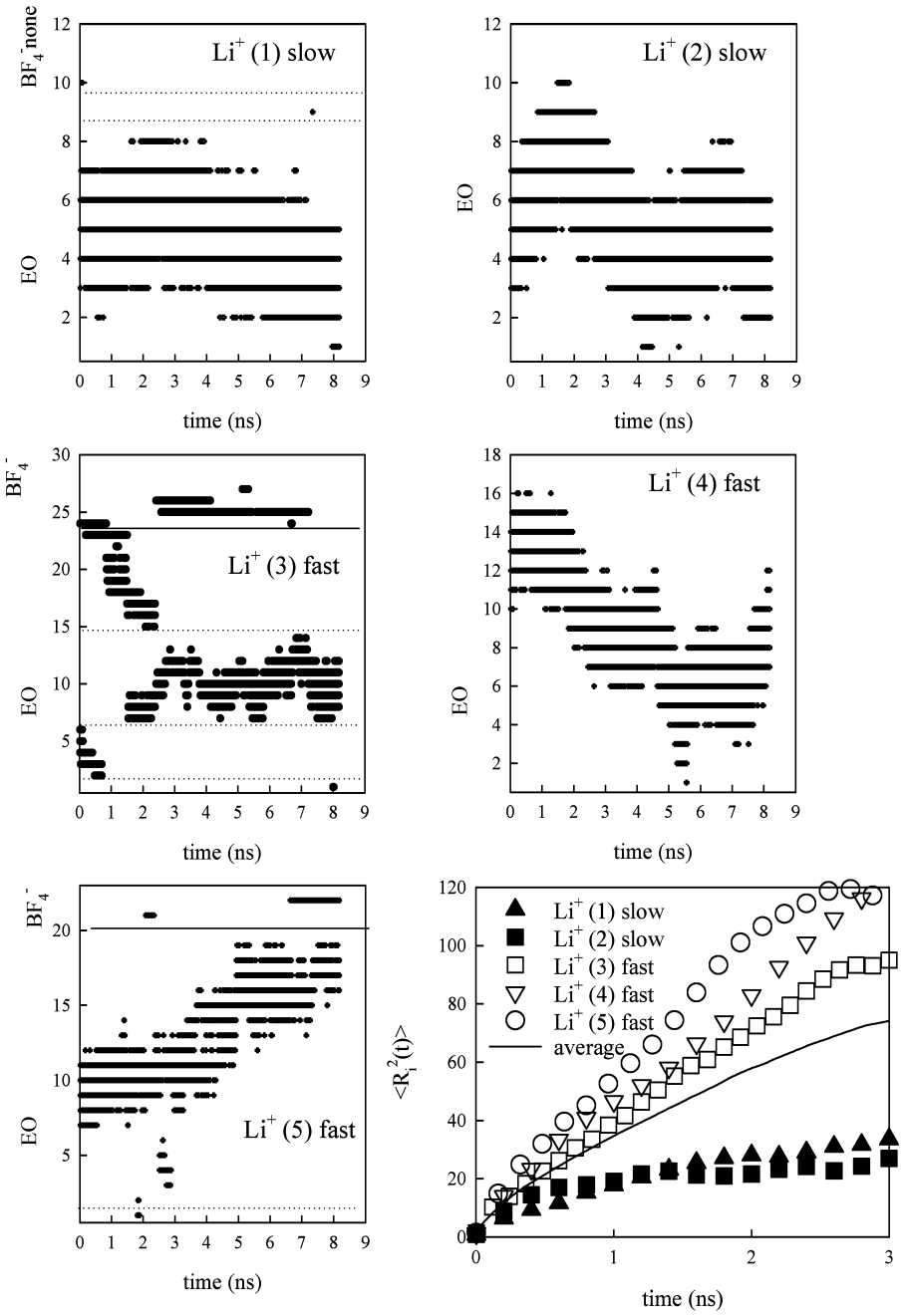

Figure 11. Li^+ environment and ion mean-squared displacements $\langle R_i(t)\rangle$ for PEO/$LiBF_4$ at 393 K with the MB force field.

the Li^+ coordination shell until its first exit, even if it exits for 1 ps and re-enters, whereas the $R_1(t)$ function probes the time that the EO atom is in the coordination shell of a Li^+ cation, regardless of how many times the EO exits and enters the Li^+ coordination shell.

The dramatic difference between the residence time correlation functions $R_1(t)$ and $R_2(t)$, shown in Figure 12, indicates that the EO atom exits and re-enters the Li^+ first coordination shell many times before it eventually leaves the Li^+ cation. The residence time correlation function $R_1(t)$ is closely associated with the Li^+ motion along a PEO chain. The long time decay of the $R_1(t)$ functions is adequately described by a single exponential with relaxation times of 13 and 37 ns for the MD simulations with the MB and TB force fields, respectively. These relaxation rates correspond to the probability of an EO atom to depart from the Li^+ environment in 28 ns for the MB force fields and 79 ns for the TB force fields. Figure 7c indicates that the most probable number of EO atoms around a Li^+ cation is 5 for MB force fields and 7 for TB force fields; therefore, we can estimate that a Li^+ cation moves five EO atoms in 28 ns for the MB force fields, and seven EO atoms in 79 ns for the TB force field. (See Figure 8 in ref 43 for the relationship between the correlation time and the probability for exiting the coordination shell.) We attempt to estimate Li^+ diffusion along the PEO chain by assuming that Li^+ cations can move along the PEO only in one direction. Using the PEO characteristic ratio of 5, we estimate that, in 1 ns, a Li^+ cation moves along the PEO chain the mean-square distance of $3 \times C_\infty nl^2$, where C_∞ is the PEO characteristic ratio, n is the number of bonds the Li^+ cation travels in 1 ns, l^2 is the mean-squared bond length ($l^2 = 2.1$ Å^2), and 3 is the number of bonds separating the EO atoms. We obtain a value of $C_\infty nl^2 = 3 \times 5 \times (5/28) \times 2.1 = 5.6$ Å^2/ns for the simulations that employ the MB force field and $C_\infty nl^2 = 2.6$ Å^2/ns for the simulations that employ the TB

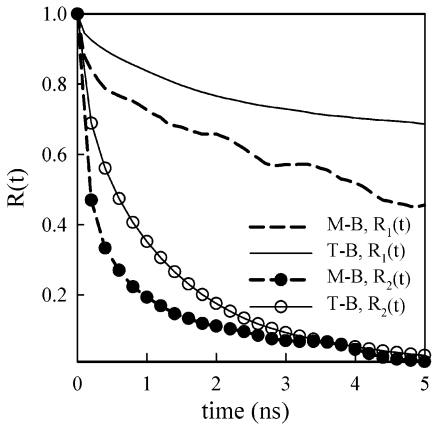

Figure 12. Residence time correlation functions $R_1(t)$ and $R_2(t)$ Li^+-EO.

force field. The "free" Li^+ self-diffusion coefficients of ~3.4 $Å^2$/ns for the MB force field and 0.8 $Å^2$/ns for the TB force field are obtained from direct analysis of the mean-square displacements of only "free" Li^+ cations. The Li^+ diffusion along the PEO chain from our model, on the basis of Li^+-EO residence times is similar, within a factor of 3, to the "free" Li^+ diffusion, which suggests a way to estimate the Li^+ diffusion coefficient from Li^+-EO residence times and vice versa.

V. Conclusions

We have presented a methodology for the development of the many-body (MB) polarizable and effective mean-field-type two-body (TB) force fields for the simulations of polymer electrolytes. The repulsion parameters for ion−PEO and cation−anion interactions were determined from the basis set superposition error (BSSE)-corrected Hartree−Fock (HF) calculations, using a relatively inexpensive aug-cc-pvDz basis set; however, a double extrapolation, for better treatment of the electron correlations, and larger basis sets were required to obtain reliable dispersion parameters. The MB polarizable force field for Li^+/PEO interactions was found to provide an accurate description of Li^+ complexation with oligomers of poly(oxymethylene), which indicates the transferability of the Li^+/PEO complex to similar compounds.

Molecular dynamics (MD) simulations have been performed on poly(ethylene oxide) (PEO) (M_w = 2380)/$LiBF_4$ polymer electrolytes (for EO:Li = 15:1, where EO represents an ether oxygen atom) at temperatures of 363, 393, and 423 K. The time scale for equilibration of these systems were investigated at 393 K by setting up systems with very different ion aggregation states, namely, a system with the majority (>80%) of ions being free ions and a system with the majority (>80%) of ions participating in ion aggregates and ion pairs. After 100-ns MD simulations of the first system and 80-ns simulations of the second system, the fraction of free Li^+ cations was different by 20% between the systems, whereas the fraction of free BF_4^- anions were different by 40% between the systems, which indicated that longer equilibration times are required to obtain the fraction of free ions with a better accuracy.

MD simulations with the MB potentials yielded information about the Li^+ environment, the extent of slowing of the PEO dynamics with the addition of salt, the ion self-diffusion coefficient, and the conductivity that agreed reasonably with the available experimental data. The two-body approximation of the MB force field was successful in predicting the fractions of Li^+ and BF_4^- free ions and ion aggregates, but it overestimated the number of EO atoms in the first coordination shell of the Li^+ cation and predicted slower PEO and ion dynamics.

The main contribution to the "free" Li^+ diffusion coefficient was found to come from Li^+ motion along the PEO chains and can be either calculated through direct analysis of the Li^+ mean-square displacements or estimated from the Li^+-EO residence time autocorrelation function. The Li^+ hopping rate from one PEO chain to another is on the order of hundreds of nanoseconds, whereas the rate of the Li^+ cation to associate or dissociate with the BF_4^- anion is on the order of tens or hundreds of nanoseconds, which is consistent with the Li^+ motion on the PEO radius of gyration length scale and then undergoing a jump to another PEO chain or joining ion aggregates. However, it is still not clear at this point what the limiting factors for cation transport are. Possible limiting factors include, but not limited to, the rate of cation hopping from one chain to another, hopping from PEO to ion aggregates, or slow cation motion along the chain between the jumps.

Acknowledgment. The authors are indebted to NASA (Grant No. NAG3 2624) and a subcontract from Lawrence Berkeley National Laboratory (LBL) (Subcontract No. 6515401) for financial support. We also would like to thank our collaborators John Kerr, David Price, Marie-Louise Saboungi, Larry Curtiss, Oleksey Byutner, Dmitry Bedrov, Sergio Petrucci, Frans Trouw, Richard Jaffe, and Michel Armand.

References and Notes

(1) Gray, F. M. *Polymer Electrolytes*; The Royal Society of Chemistry: Cambridge, U.K., 1997.

(2) Bruce, P. G.; Vincent, C. A. Polymer Electrolytes. *J. Chem. Soc., Faraday Trans.* **1993**, *89*, 3187−3203.

(3) Bertier, C.; Gorecki, W.; Minier, M.; Armand, M. B.; Chabagno, J. M.; Gigaus, P. *Solid State Ionics* **1983**, *11*, 91.

(4) Borodin, O.; Smith, G. D. *Macromolecules* **1998**, *31*, 8396.

(5) Londono, J. D.; Annis, B. K.; Habenschuss, A.; Borodin, O.; Smith, G. D.; Turner, J. Z.; Soper, A. K. *Macromolecules* **1997**, *30*, 7151.

(6) Ratner, M. A.; Shriver, D. F. *Chem. Rev.* **1988**, *88*, 109.

(7) Nitzan, A.; Ratner, M. A. *J. Phys. Chem.* **1994**, *98*, 1765.

(8) Furukawa, T.; Imura, M.; Yuruzume, H. *Jpn. J. Appl. Phys.* **1997**, *36*, 1119.

(9) Buriez, O.; Han, Y. B.; Hou, J.; Kerr, J. B.; Qiao, J.; Sloop, S. E.; Tian, M.; Wang, S. *J. Power Sources* **2000**, *89*, 149.

(10) Allcock, H. R.; Napierala, M. E.; Olmeijer, D. L.; Cameron, C. G.; Kuharcik, S. E.; Reed, C. S.; O'Connor, S. J. M. *Electrochim. Acta* **1998**, *43*, 1145.

(11) Müller-Plathe, F. *Acta Polym.* **1994**, *45*, 259.

(12) Müller-Plathe, F.; van Gunsteren, W. F. *J. Chem. Phys.* **1995**, *103*, 4745.

(13) Neyertz, S.; Brown, D. *J. Chem. Phys.* **1996**, *104*, 3797.

(14) Mos, B.; Verkerk, P.; Pouget, S.; van Zon, A.; Bel, G.-J.; de Leeuw, S. W.; Eisenbach, C. D. *J. Chem. Phys.* **2000**, *113*, 4.

(15) Halley, J. W.; Duan, Y.; Curtiss, L. A.; Baboul, A. G. *J. Chem. Phys.* **1999**, *111*, 3302.

(16) Boinske, P. T.; Curtiss, L.; Halley, J. W.; Lin, B.; Sutjianto, A. *J. Comput.-Aided Mater. Des.* **1996**, *3*, 385.

(17) Hyun, J.-K.; Dong, H.; Rhodes, C. P.; Frech, R.; Wheeler, R. A. *J. Phys. Chem. B* **2001**, *105*, 3329.

(18) Borodin, O.; Smith, G. D. *Macromolecules* **2000**, *33*, 2273.

(19) Smith, G. D.; Jaffe, R. L.; Partridge, H. *J. Phys. Chem. A* **1997**, *101*, 1705.

(20) Borodin, O.; Smith, G. D.; Jaffe, R. L. *J. Comput. Chem.* **2001**, *22*, 641.

(21) de Jonge, J. J.; van Zon, A.; de Leeuw, S. W. *Solid State Ionics* **2002**, *147*, 349.

(22) Borodin, O.; Smith, G. D. *J. Phys. Chem. B*, **2003**, *107*, 6801.

(23) Borodin, O.; Douglas, R.; Smith, G. D.; Trouw, F.; Petrucci, S. *J. Phys. Chem. B*, **2003**, *107*, 6813.

(24) Dunning, T. H. *J. Chem. Phys.* **1987**, *98*, 1007.

(25) Krishman, R.; Binkley, J. S.; Seeger, R.; Pople, J. A. *J. Chem. Phys.* **1980**, *72*, 650.
(26) Frisch, M. J.; Trucks, G. W.; Schlegel, H. B.; Scuseria, G. E.; Robb, M. A.; Cheeseman, J. R.; Zakrzewski, V. G.; Montgomery, J. A., Jr.; Stratmann, R. E.; Burant, J. C.; Dapprich, S.; Millam, J. M.; Daniels, A. D.; Kudin, K. N.; Strain, M. C.; Farkas, O.; Tomasi, J.; Barone, V.; Cossi, M.; Cammi, R.; Mennucci, B.; Pomelli, C.; Adamo, C.; Clifford, S.; Ochterski, J.; Petersson, G. A.; Ayala, P. Y.; Cui, Q.; Morokuma, K.; Malick, D. K.; Rabuck, A. D.; Raghavachari, K.; Foresman, J. B.; Cioslowski, J.; Ortiz, J. V.; Stefanov, B. B.; Liu, G.; Liashenko, A.; Piskorz, P.; Komaromi, I.; Gomperts, R.; Martin, R. L.; Fox, D. J.; Keith, T.; Al-Laham, M. A.; Peng, C. Y.; Nanayakkara, A.; Gonzalez, C.; Challacombe, M.; Gill, P. M. W.; Johnson, B. G.; Chen, W.; Wong, M. W.; Andres, J. L.; Head-Gordon, M.; Replogle, E. S.; Pople, J. A. *Gaussian 98*, revision A.7; Gaussian, Inc.: Pittsburgh, PA, 1998.
(27) Becke, A. D. *J. Chem. Phys.* **1993**, *98*, 5648. Perdew, J. P.; Chevary, J. A.; Vosko, S. H.; Jackson, K. A..; Pederson, M. R.; Singh, D. J.; Fiolhais, C. *Phys. Rev. B* **1992**, *46*, 6671.
(28) Borodin, O.; Bell, R. L.; Li, Yi; Bedrov, D.; Smith, G. D. *Chem. Phys. Lett.* **2001**, *336*, 292−302.
(29) Sutjianto, A.; Curtiss, L. A. *J. Phys. Chem. A* **1998**, *102*, 968.
(30) Lide, D. R., Ed. *CRC Handbook of Chemistry and Physics*, 81st ed.; CRC Press: Boca Raton, FL, 2000.
(31) Nose, S. In *Computer Simulation in Materials Science*; Meyer, M., Pontikis, V., Eds.; Kluwer Academic Publishers, Amsterdam, 1991; p 21.
(32) Martyna, G. J.; Tuckerman, M.; Tobias, D. J.; Klein, M. L. *Mol. Phys.* **1996**, *87*, 1117.
(33) Ryckaert, J. P.; Ciccotti, G.; Berendsen, H. J. C. *J. Comput. Phys.* **1977**, *23*, 327.
(34) Deserno, M.; Holm, C. *J. Chem. Phys.* **1998**, *109*, 7678.
(35) Steinhauser, O. *Mol. Phys.* **1982**, *45*, 335.
(36) Martyna, G. J.; Tuckerman, M.; Tobias, D. J.; Klein, M. L. *Mol. Phys.* **1996**, *87*, 1117.
(37) Bedrov, D.; Smith, G. D. *J. Chem. Phys.* **2001**, *115*, 1121.
(38) Mao, G.; Saboungi, M.-L.; Price, D. L.; Armand, M.; Howells, W. S. *Phys. Rev. Lett.* **2000**, *84*, 5536.
(39) Arumugam, S.; Shi, J.; Tunstall, D. P.; Vincent, C. A. *J. Phys.: Condens. Matter* **1993**, *5*, 153.
(40) Shi, J.; Vincent, C. A. *Solid State Ionics* **1993**, *60*, 11.
(41) Sun, H. Y.; Takeda, Y.; Imanishi, N.; Yamamoto, O.; Sohn, H.-J. *J. Electrochem. Soc.* **2000**, *147*, 2462.
(42) Lee, J. Y.; Liu, Y.; Hong, L. Presented at the 11th International Meeting on Lithium Batteries (IMLB 11), Monterey, CA, June 23−28, 2002; Abstract 179.
(43) Smith, G. D.; Borodin, O.; Bedrov, D.; Paul, W.; Qiu, X.; Ediger, M. D. *Macromolecules* **2001**, *34*, 5192.